

Numerical experiments in idealized glacier topographies

Case study of the impact of the mesh resolution on the prediction of the grounding line position

Ruben ESPELETA BOLIVAR

Advisor: Dr. Cruz GARCÍA MOLINA

¹Institut des geosciences de l'environnement

May 24th, 2023

- 1 Introduction
- 2 Glacier dynamics
- 3 Grounding line dynamics and stability
- 4 Numerical model
- 5 Systems and experiment set-up
- 6 Numerical parameters
- 7 Results
- 8 Conclusions

What is a glacier?

Glaciers can be defined as a mass of ice that accumulates from snow and flows downwards from a few hundreds of meters per year and up to 15 km per year.

What is a glacier?

Glaciers can be defined as a mass of ice that accumulates from snow and flows downwards from a few hundreds of meters per year and up to 15 km per year.

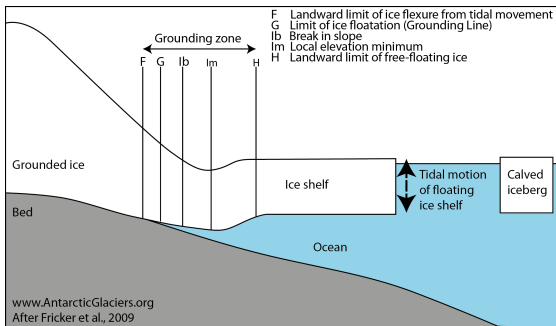


Figure: Schema of a tributary glacier where we can observe the different parts denoting the grounding zone Adapted from Fricker et al. (2009).

Importance of understanding the dynamics of glaciers

- The rate of present-day sea-level rise has increased in recent decades and it is expected to continue increasing in coming decades and centuries (Clark et al., 2015).

Importance of understanding the dynamics of glaciers

- The rate of present-day sea-level rise has increased in recent decades and it is expected to continue increasing in coming decades and centuries (Clark et al., 2015).
- Mass loss from glaciers is strongly linked to changes in the ice shelves and their grounding lines (Brunt et al., 2010; Pritchard et al., 2012).

Importance of understanding the dynamics of glaciers

- The rate of present-day sea-level rise has increased in recent decades and it is expected to continue increasing in coming decades and centuries (Clark et al., 2015).
- Mass loss from glaciers is strongly linked to changes in the ice shelves and their grounding lines (Brunt et al., 2010; Pritchard et al., 2012).
- Ice thinning and rising sea levels can cause grounding line to retreat while thickening or declining sea levels can cause an advance (Friedl et al., 2020).

Glacier flow



Figure: Glaciers behave as a very viscous fluid for time scales between a few years to a few thousands of years.

Governing equations I

- The plastic lower ice of the glacier can flow like a very viscous fluid. The incompressibility condition leads to:

$$\nabla \cdot u = 0. \quad (1)$$

- For ice flow, the acceleration term can be neglected in the Navier-Stokes equations (Hutter, 1982). Therefore:

$$-\nabla \cdot p + \nabla \cdot (\eta(\nabla \cdot u + (\nabla \cdot u)^T)) + \rho g = 0. \quad (2)$$

Where η is the viscosity and g is the gravity.

- Letting σ denote the stress tensor and pressure p is the mean normal stress denoted previously, and the strain rate tensor ϵ_e , related by:

$$\sigma = 2\eta\epsilon_e - pI = \eta \cdot (\nabla \cdot u + (\nabla \cdot u)^T) - pI. \quad (3)$$

Where I is the identity tensor. Together, these two last mathematical equations are called the full-stokes model.

The flow law

The most commonly used flow law for ice is Glen's flow law, named after John W. Glen upon whose experiments it is based Glen (1958). This equation was originally written in the form:

$$\dot{\epsilon}_e = \left(\frac{\sigma_e}{B}\right)^n; \quad (4)$$

where B is a viscosity parameter that increases as the ice becomes stiffer, and n is an empirically determined constant. Most studies have found that $n=3$. An alternative form of the flow law that is commonly used, and that can be used, is:

$$\dot{\epsilon}_e = A\sigma_e^n \quad (5)$$

A is called the rate factor. B is normally given in $\text{MPa yr}^{\frac{1}{n}}$ while A is in $\text{MPa}^{-n} \text{ yr}^{-1}$ or $\text{MPa}^{-n} \text{ s}^{-1}$.

Boundary conditions and time evolution I

- Ice in contact with the bedrock: Weertman sliding law (Weertman, 1974):

$$u_b = C\tau_b^m; \quad (6)$$

- The ice surface is assumed stress free $\sigma \cdot n = 0$ and ice base at z_s and z_b behave as free surfaces according to:

$$\frac{\delta z_i}{\delta t} + u_i \frac{\delta z_i}{\delta x} + v_i \frac{\delta z_i}{\delta y} = w_i + a_i; \quad (7)$$

where a_i is the accumulation ($a_i > 0$) or ablation ($a_i < 0$) in meter ice equivalent per year, and i = surface or base, respectively.

- By vertical integration of the incompressibility condition, w can be eliminated:

$$\frac{\delta H}{\delta t} + \frac{\delta H \bar{u}}{\delta x} + \frac{\delta H \bar{v}}{\delta y} = a_s - a_b;$$

Where \bar{u} and \bar{v} are the vertically integrated horizontal velocities.

- For the ice-ocean interface, the ice flux out of the domain will be fixed as the calving rate.

Shallow shelf approximation

SSA approximation has been derived by dimensional analysis based on a small aspect ratio between vertical and longitudinal length of the ice shelf. The conservation of momentum simplifies to:

$$\nabla_h \cdot (2\bar{\eta}(\dot{\epsilon}_h I)) = \rho g H \nabla_h \cdot \mathbf{z}_s; \quad (9)$$

Where the subscript h represents the components in the x - y plane and $\bar{\eta}$ the vertically integrated viscosity. The effective strain rate simplifies to:

$$\dot{\epsilon}_h = \sqrt{\frac{\delta u^2}{\delta x^2} + \frac{\delta v^2}{\delta y^2} + \frac{\delta u}{\delta x} \frac{\delta v}{\delta y} + \frac{1}{4} \left(\frac{\delta u}{\delta y} + \frac{\delta v}{\delta x} \right)^2}; \quad (10)$$

Grounding line dynamics and stability

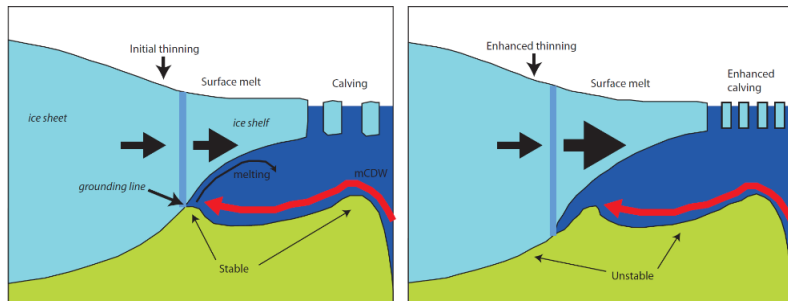


Figure: Schematic representation of the marine ice sheet instability with an initial stable grounding line position (left hand side) and unstable grounding line position after the incursion of warm circumpolar deep water below the ice shelf. Adapted from Hanna et al. (2013).

Process of modelling

The physical phenomena that impacts the dynamics of the glaciers can be represented using mathematical models that implement partial differential equations, which can then be discretized to be solved using numerical methods.

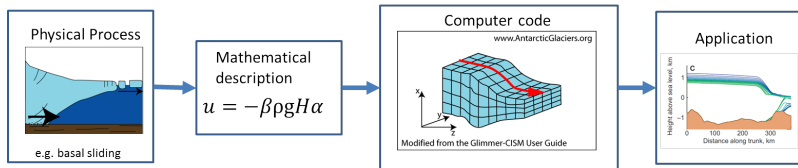


Figure: Process of modelling, starting with a physical phenomena which can be represented mathematically in a physical model than can then be discretized to solve numerically. Adapted from AntarcticGlaciers.org

- Open source finite element code, mainly developed in Finland.
- The ice sheet/ice flow model Elmer/Ice is based on Elmer and includes developments related to glaciological problems. It includes a large number of dedicated solvers and users functions.
- Elmer/Ice solves the Stokes equations and it includes solvers for the approximations of the Stokes equations, namely shallow shelf and shallow ice approximations.

The intercomparison project (<https://github.com/JRowanJordan/CalvingMIP>) is intended to develop models to explore calving, ice damage, and glacier dynamics leading to recommendations for improved calving laws in ice sheet models.

Cone domain

The idealised experimental domain comprise a simple, symmetrically circular domain. This first idealized model consists of a circular bedrock configuration (Figure 5) given by:

$$Bed_0 = Bc - (Bc - Bl) \frac{|x^2 + y^2|}{r^2}; \quad (11)$$

Where $r=800 \times 10^3 \text{m}$, $Bc=0.9 \times 10^3 \text{m}$, and $Bl=-2 \times 10^3 \text{m}$.

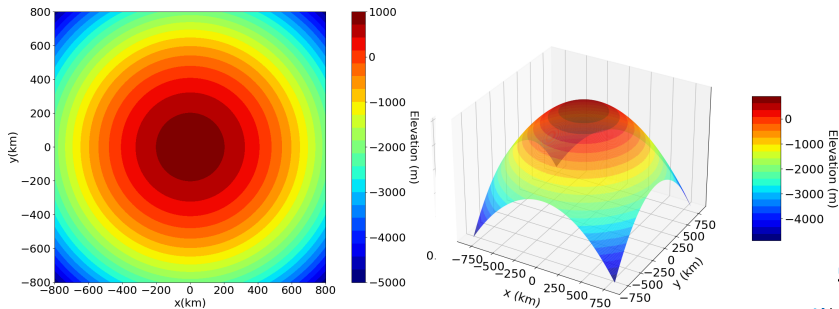


Figure: Circular bedrock topography. On the left side top view and on the right side, lateral view.

Experimental profiles

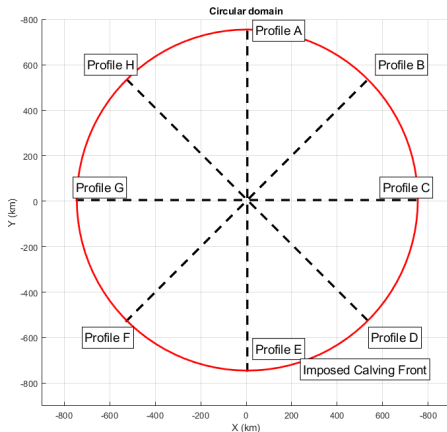


Figure: Circular domain experimental profiles as well as the initial imposed calving front position. Adapted from CalvingMIP inter-comparison project.

The Thule bedrock configuration is shown in Figure 7 and is given by:

$$\theta = \arctan2(y, x); \quad (12)$$

$$l = r - \cos(2\theta) \frac{r}{2}; \quad (13)$$

$$Bed_0 = Bc - (Bc - Bl) \frac{|x^2 + y^2|}{r^2}; \quad (14)$$

$$Bed = Bacos(3\pi \frac{\sqrt{x^2 + y^2}}{l}) + Bed_0; \quad (15)$$

With $r=800 \times 10^3 m$, $Bc=0,9 \times 10^3 m$, $Bl=-2 \times 10^3 m$, and $Ba=1.1 \times 10^3 m$.

Thule domain bedrock topography

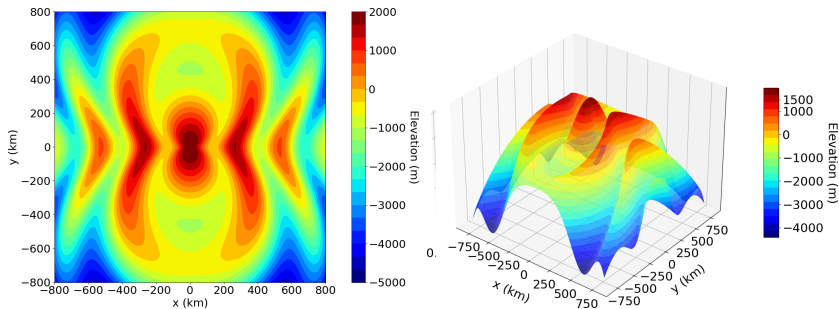


Figure: Thule bedrock topography 3D. On the left side the top view, and on the right side a lateral view.

Thule experimental profiles

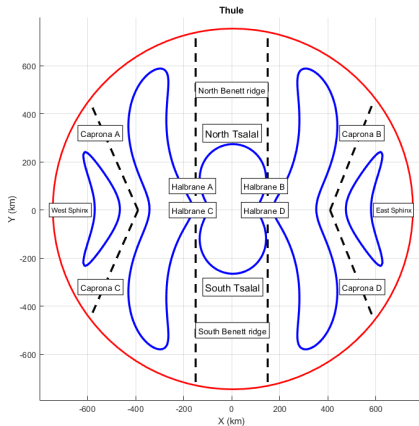


Figure: Thule domain experimental profiles as well as the initial imposed calving front position. Adapted from CalvinMIP inter-comparison project.

Table: Physical parameters

Variable	Description	Units
$g = 9.81$	Gravitational acceleration	ms^{-2}
$a_s = 0.3$	Surface mass balance (SMB)	ma^{-1}
$a_b = 0$	Basal mass balance (BMB)	ma^{-1}
$\rho_i = 917$	Ice density	kg m^{-3}
$\rho_w = 1028$	Sea water density	kg m^{-3}
$A = 2.9377 \times 10^{-9}$	Ice rate factor	$\text{KPa}^{-3} \text{a}^{-1}$
$n = 3$	Flow law stress exponent	Dimensionless
$C = 0.001$	basal slipperiness	$\text{ma}^{-1} \text{KPa}^{-3}$
$m = 3$	Sliding law stress exponent	Dimensionless
$s2a = 31556926$	Seconds in a year	s

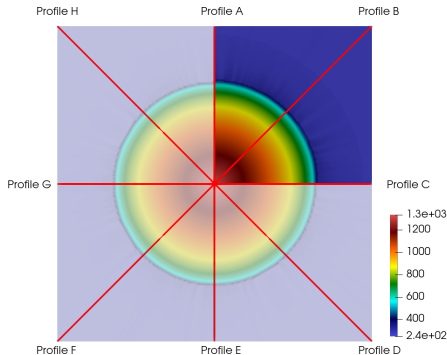
Numerical variables, external forcings and initial condition

- The numerical resolution will be the variable parameter, varying from 10km, 5km, 2km, and 1km.
- The external forces acting will be gravity, as well as the ice friction and the basal stress.
- The initial condition will be a topography with no ice, namely $h_0=0\text{m}$.
- The CFL condition will be necessary to verify the stability of the model. It is needed that:

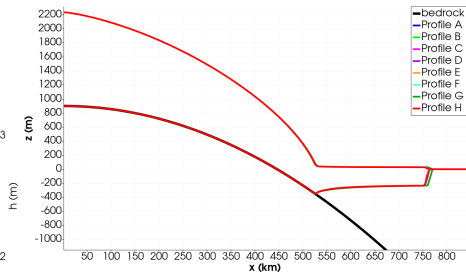
$$C = \frac{u\Delta t}{\Delta x} < C_{max}; \quad (16)$$

where, C is the Courant number, u is the velocity, Δt is the time step, Δx is the horizontal resolution. $C_{max} = 1$ is a safe approximation.

Results:Cone ice thickness



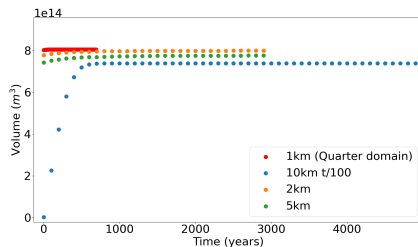
(a) Profiles for Cone circular domain



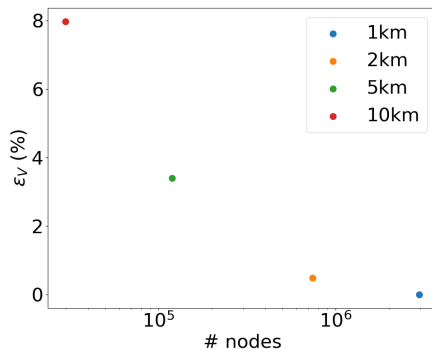
(b) Ice thickness per profile

Figure: Circular domain ice sheet showing the ice thickness results along the profiles proposed.

Volume variation in time and per number of nodes



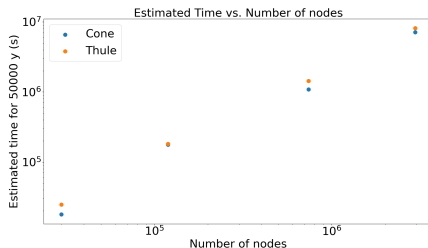
(a) Volume variation in time.



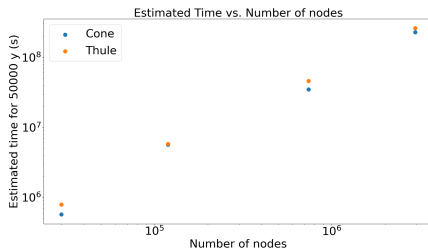
(b) Volume relative variation as a function of the number of nodes.

Figure: Volume variation in time and per number of nodes for the cone experiment.

Simulations time as a function of the number of nodes



(a) Time for 32 processors used.



(b) Time for 1 processor.

Figure: Simulation time as a function of the number of nodes for each resolution mesh.

Grounding line position per resolution

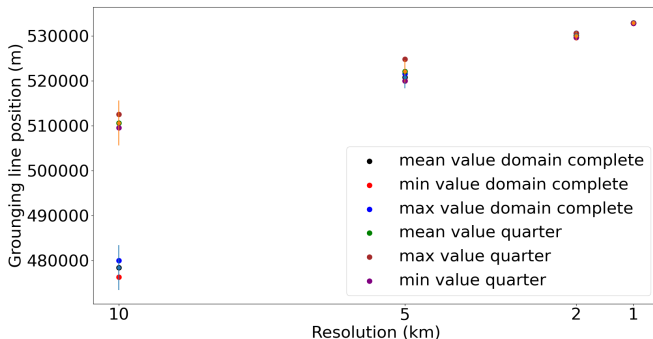


Figure: Grounding line positions as a function of the resolution for quarter and complete circular cone domain.

Results: Thule domain I

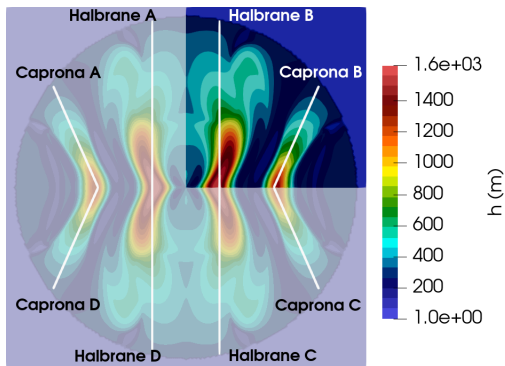
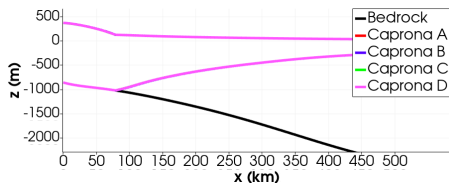
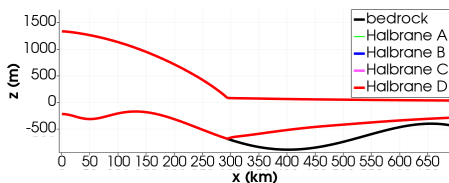


Figure: Profiles for the thule domain

Results: Thule domain II



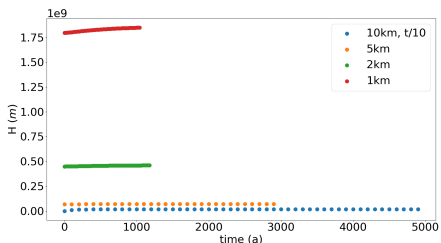
(a) Ice thickness along each Caprona profiles.



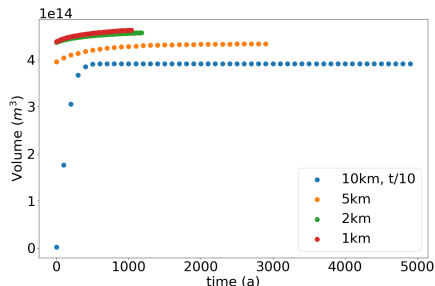
(b) Ice thickness along each Halbrane profiles.

Figure: Ice thickness along the thule domain profiles.

Results: Thule domain III



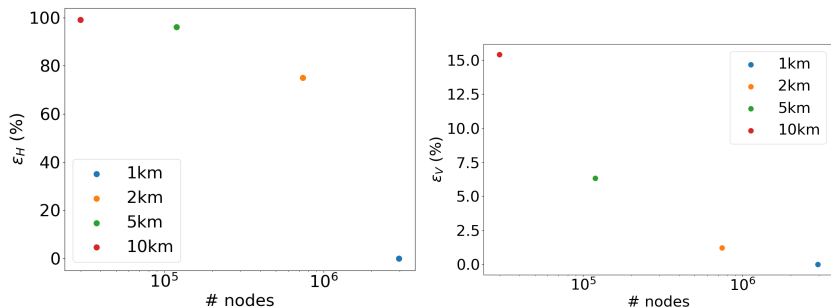
(a) Ice thickness variation in time.



(b) Volume variation in time.

Figure: Ice thickness and volume variation in time for the Thule domain experiment.

Results: Thule domain IV

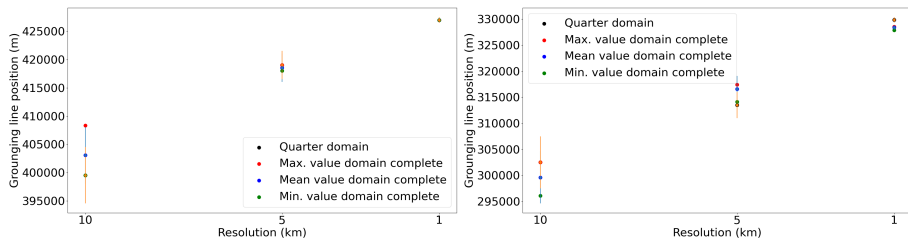


(a) Ice thickness error as a function of the number of nodes.

(b) Volume relative variation as a function of the number of nodes.

Figure: Volume and ice thickness variation as a function of the number of nodes for the thule domain experiment.

Results: Thule domain V



(a) Grounding line positions along Capronas profiles. (b) Grounding line positions along Halbrane profiles.

Figure: Grounding line positions as a function of the resolution for quarter and complete thule domain along the Caprona and Halbrane profiles.

- The grounding line position is increasing as a function of the resolution, due to the topography of both experiments.
- The fact that the grounding line position increases in a higher resolution, means that the ice thickness will also increase, since the ice column at the grounding line is now larger due to the decreasing slope of the bedrock, meaning that the ice flux through the grounding line will increase.
- The resolution has a direct impact in the symmetry of the domain of study, leading to differences in results of parts of the domain if the resolution is low.

Bibliography and references I

- Brunt, K. M., Fricker, H. A., Padman, L., Scambos, T. A., and O'Neel, S. (2010). Mapping the grounding zone of the ross ice shelf, antarctica, using icesat laser altimetry. *Annals of Glaciology*, 51(55):71–79.
- Clark, P. U., Church, J. A., Gregory, J. M., and Payne, A. J. (2015). Recent progress in understanding and projecting regional and global mean sea level change. *Current Climate Change Reports*, 1(4):224–246.
- Durand, G., Gagliardini, O., Zwinger, T., Le Meur, E., and Hindmarsh, R. C. (2009). Full stokes modeling of marine ice sheets: influence of the grid size. *Annals of Glaciology*, 50(52):109–114.
- Fricker, H. A., Coleman, R., Padman, L., Scambos, T. A., Bohlander, J., and Brunt, K. M. (2009). Mapping the grounding zone of the amery ice shelf, east antarctica using insar, modis and icesat. *Antarctic Science*, 21(5):515–532.

Bibliography and references II

- Friedl, P., Weiser, F., Fluhrer, A., and Braun, M. H. (2020). Remote sensing of glacier and ice sheet grounding lines: A review. *Earth-Science Reviews*, 201:102948.
- Glen, J. (1958). The flow law of ice: A discussion of the assumptions made in glacier theory, their experimental foundations and consequences. *IASH Publ*, 47(171):e183.
- Hanna, E., Navarro, F., Pattyn, F., Domingues, C., Fettweis, X., Ivins, E., Nicholls, R., Ritz, C., Smith, B., and Tulaczyk, S. (2013). White-25 house, pl, and zwally, hj: Ice-sheet mass balance and climate change. *Nature*, 498:51–59.
- Hooke, R. L. (2019). *Principles of glacier mechanics*. Cambridge university press.
- Hutter, K. (1982). A mathematical model of polythermal glaciers and ice sheets. *Geophysical & Astrophysical Fluid Dynamics*, 21(3-4):201–224.

- Pritchard, H., Ligtenberg, S. R., Fricker, H. A., Vaughan, D. G., van den Broeke, M. R., and Padman, L. (2012). Antarctic ice-sheet loss driven by basal melting of ice shelves. *Nature*, 484(7395):502–505.
- Weertman, J. (1974). Stability of the junction of an ice sheet and an ice shelf. *Journal of Glaciology*, 13(67):3–11.